High-order and tunable balanced bandpass filters using mixed technology resonators

Dakotah Simpson [iD] and Dimitra Psychogiou

Department of Electrical, Computer, and Energy Engineering, University of Colorado Boulder, Boulder, CO, USA

CAMBRIDGE UNIVERSITY PRESS

Abstract

This paper reports on high-order balanced bandpass filters (BPFs) that are continuously tunable in terms of frequency and bandwidth and can be intrinsically switched-off. They use a hybrid integration scheme based on two different types of capacitively loaded resonators—ceramic coaxial and microstrip—that reduce the filter size, enhance its out-of-band selectivity and common-mode suppression, and allow for multiple levels of transfer function tuning. High selectivity is obtained in the differential mode due to the high number of poles and transmission zeros present. The common mode is highly suppressed through the introduction of additional transmission zeros and resistively loaded resonators. Furthermore, the use of ceramic coaxial resonators results in supplementary transmission zeros that are used to lower the out-of-band transmission in the differential mode. Multiple levels of tuning are obtained by reconfiguring only the frequency of the BPF's resonators. For experimental validation, a tunable mixed-technology microstrip prototype was manufactured and measured at S-band. It exhibited frequency tuning between 2.22 and 2.94 GHz, bandwidth tuning between 104 and 268 MHz, and an intrinsically switched-off mode with isolation >50 dB in the differential mode. For all states, the common mode was suppressed by at least 35 dB at the center frequency and within a wide range.

Introduction

Balanced radio frequency (RF) transceivers offer the advantage of higher immunity, which is important in maintaining a high signal-to-noise ratio in the RF front-end, to electromagnetic (EM) interference, crosstalk, and other types of noise [1]. Balanced front-ends with the ability to adapt to different communication bands and suppress a variety of interfering signals have been of importance in multi-standard RF transceivers. As a key component in such systems, tunable balanced bandpass filters (BPFs) that efficiently transmit the signals in the differential mode and effectively suppress signals in the common mode have been a focus of recent research efforts [2–13]. Although a number of tunable concepts have been presented in the open technical literature [2–9], the majority of them focus on center frequency tuning only. For example, a balanced BPF is designed with the use of open-loop resonators in [2]. Despite producing tunable transmission zeros (TZs) with the purpose of increasing selectivity, its second-order transfer function has limited selectivity near the passband. The balanced BPF in [3] was designed using substrate-integrated waveguide dual-mode cavity resonators and exhibits limited tunability (only tunable in frequency), low levels of common-mode suppression (30 dB), and poor differential mode selectivity (second-order response). Magnetically coupled stepped-impedance resonators are used in [4]. Similar to the other filters, this design demonstrates low selectivity (second-order response), low levels of common-mode suppression (20 dB), and limited levels of tuning (only tunable in bandwidth (BW)). A variety of coupled microstrip line balanced BPFs are presented in [5–9]. However, their shortcomings include center frequency tuning only and low selectivity (first order in [5], second order in [6–8], and third order in [9]).

Only very few fully-reconfigurable balanced BPFs have been presented to date. For example, the second-order balanced BPF in [10] is implemented with coupled-line resonators and shows low levels of selectivity in its differential mode (only two poles). Furthermore, it lacks the ability to suppress the common mode with suppression levels of ~40 dB within the differential mode passband. The balanced BPF presented in [11] makes use of compact multi-mode resonators which results in a second-order differential mode transfer function that is tunable in both center frequency and BW. However, the filter does not effectively suppress the common mode (suppression of ~20 dB) and produces narrow levels of BW tuning (2.2:1). The BPFs presented in this work are an extension of the fully reconfigurable BPF in [12], where microstrip resonators and impedance inverters are used in the balanced network to create a fully reconfigurable balanced BPF with higher selectivity. The aim of this paper is to improve the selectivity and out-of-band rejection by increasing the order of the filter and to implement electronic tuning by using varactor diodes. Furthermore, this manuscript explores

the fully reconfigurable balanced BPF concept and architecture capabilities in more depth through a generalized filter concept and physical implementation studies.

Taking into consideration the limitations of the state of the art, a new class of quasi-elliptic fully reconfigurable balanced BPFs with high selectivity and high common-mode suppression is reported. The differential mode is shaped by an arbitrary number of TZs and poles and can be tuned in terms of BW and center frequency and can be intrinsically switched off (i.e., without the use of RF switches). To further increase the selectivity and suppress spurious resonance modes, a hybrid integration technique using ceramic coaxial and microstrip resonators is considered. An earlier version of this paper was presented at the 2020 European Microwave Conference [13]. This manuscript is organized as follows. The balanced BPF concept and its corresponding tuning capabilities and practical physical design aspects are introduced in "Theoretical foundations" section through the use of coupled-resonator synthesis. "Experimental validation" section details the design of a high-order mixed integration prototype that was designed and measured at S-band. In the last section, the contributions of this work are presented in detail.

Theoretical foundations

Operating principles and tuning capabilities

The fully reconfigurable, high-order balanced BPF concept is depicted in Fig. 1. In particular, Fig. 1(a) shows the coupling–routing diagram (CRD) of the overall balanced BPF architecture. It is comprised of two input nodes (S and S′) connected together through two impedance inverters. Similarly, there are two output nodes (L and L′) that are joined through two impedance inverters and are coupled to the two input nodes through an arbitrary number (K) of resonant sections. As is shown in Fig. 1(a), each resonant section can either be a transmission pole cell (TPC) or a multi-resonant cell (MRC). The overall filter architecture is made of M TPCs and N MRCs, where $K = M + N$ is the order of the filter. A TPC consists of four non-resonating nodes and two frequency tunable resonators, which are linked and resistively loaded at the line of symmetry and result in one pole in the differential mode of operation. An MRC is composed of two isolated branches, one in series from input S to output L and the other in series from input S′ to output L′. Each branch has two tunable resonators connected together through impedance inverters and a non-resonating node. The MRC results in two tunable TZs and one pole in each mode of operation. Figures 1(b)–1(e) demonstrate the variety of transfer functions that can be obtained from the high-order balanced BPF in Fig. 1(a). As it can be seen, the filter results in K poles and $2N$ TZs in the differential mode of operation and $2N + 2$ TZs in the common mode of operation, two of which are located at the center of the passband. The TZs can be positioned to change the out-of-band characteristics of the filter's response. For example, they can all be placed near the passband for higher selectivity, as in Fig. 1(b), or symmetrically spread out, as in Fig. 1(c). Furthermore, the TZs can be arbitrarily located so that the out-of-band response is tailored to any application, which is demonstrated in Fig. 1(d). Lastly, all of the TZs can be tuned to the same frequency to intrinsically switch off the filter, which is demonstrated in Fig. 1(e).

To further elaborate on the high-order balanced BPF concept, a fifth-order design ($K = 5$) with three TPCs ($M = 3$) and two MRCs ($N = 2$) is considered in Fig. 2. Figure 2(a) depicts the overall BPF CRD, whereas Figs 2(b) and 2(c) represent the single-ended CRD equivalents of the filter under differential-mode and common-mode excitations, respectively. Figures 2(d) and 2(e) exhibit the conceptual responses of the differential and common modes of operation, respectively, where the single-ended CRDs are used as a reference.

The balanced filter behaves differently depending on the signals imparted on it. For example, when it is excited by two signals that are out of phase with another, the filter operates in the differential mode. Under the differential mode of operation, the line of symmetry that divides the filter (see Fig. 2(a)) acts as a virtual ground (i.e., short circuit), and thus can be represented by the single-ended CRD in Fig. 2(b). More specifically, the presence of the virtual ground shorts the resistors along the line of symmetry, so they are neglected in the differential mode of operation. Secondly, the virtual ground shorts (at the locations of nodes 12 and 13) the impedance inverters that connect the two inputs and the two outputs. The shorted impedance inverters act as all-pass networks and can be omitted in the CRD equivalent. Lastly, nodes 2, 6, and 10 in Fig. 2(a) are replaced by their more-compact equivalent, a single resonant node, in both (Figs 2(b) and 2(c)). Figure 2(d) shows that, in the differential mode of operation, each of the in-line resonating nodes (nodes 2, 6, and 10) introduce one frequency-tunable pole (P_1, P_3, and P_5) that is located at the center of the passband. Furthermore, nodes 3–5 (and nodes 7–9) create a network that results in two frequency-tunable TZs, TZ_1 and TZ_2 (TZ_3 and TZ_4 for nodes 7–9), and one pole, P_2 (P_4 for nodes 7–9). The spectral locations of TZ_1 and TZ_2 are equal to the resonant frequencies of nodes 4 and 5, whereas the spectral location of pole P_2 is determined by the frequency at which the two input admittances looking towards nodes 4 and 5 from node 3 cancel out. Therefore, the differential mode results in a total of four TZs and five poles, as is corroborated by Fig. 2(d).

When common-mode signals (i.e., signals that are in phase with each other) are imparted on the balanced filter, the line of symmetry behaves as a virtual open circuit and the resulting filter can be modelled with the single-ended CRD in Fig. 2(c). Under common-mode operation, the resistors loaded along the line of symmetry will be present and will introduce loss to nodes 2, 6, and 10. The added loss to these resonators weakens the presence of the poles that are introduced by them. Moreover, the virtual open circuit results in two open-ended impedance inverters at the locations of nodes 12 and 13, which in-turn introduce additional TZs. These TZs, TZ_5, and TZ_6, are unique to the common mode and improve its suppression at the center frequency of the filter by cancelling out the effect of poles P_2 and P_4. The open-ended impedance inverters are represented as resonating nodes 12 and 13 in the CRD of Fig. 2(c). In total, the common-mode response results in six TZs, two of which are unique to the common mode.

The proposed balanced BPF can be reconfigured by varying the resonant frequencies of its constituent resonators. These tuning capabilities are manifested in the various synthesized transfer functions of Fig. 3. The transfer functions were generated using the single-ended CRD equivalents in (Figs 2(b) and 2(c)) and the coupling coefficients listed in Table 1. The high levels of common-mode suppression (∼40 dB throughout the entire passband) and a highly-selective differential mode response are demonstrated in Fig. 3(a). Center frequency tuning is exhibited in Fig. 3(b) and is obtained by tuning the resonant frequencies of all resonators simultaneously. Next, Fig. 3(c) shows that the BW of the BPF can be altered by only adjusting the resonant
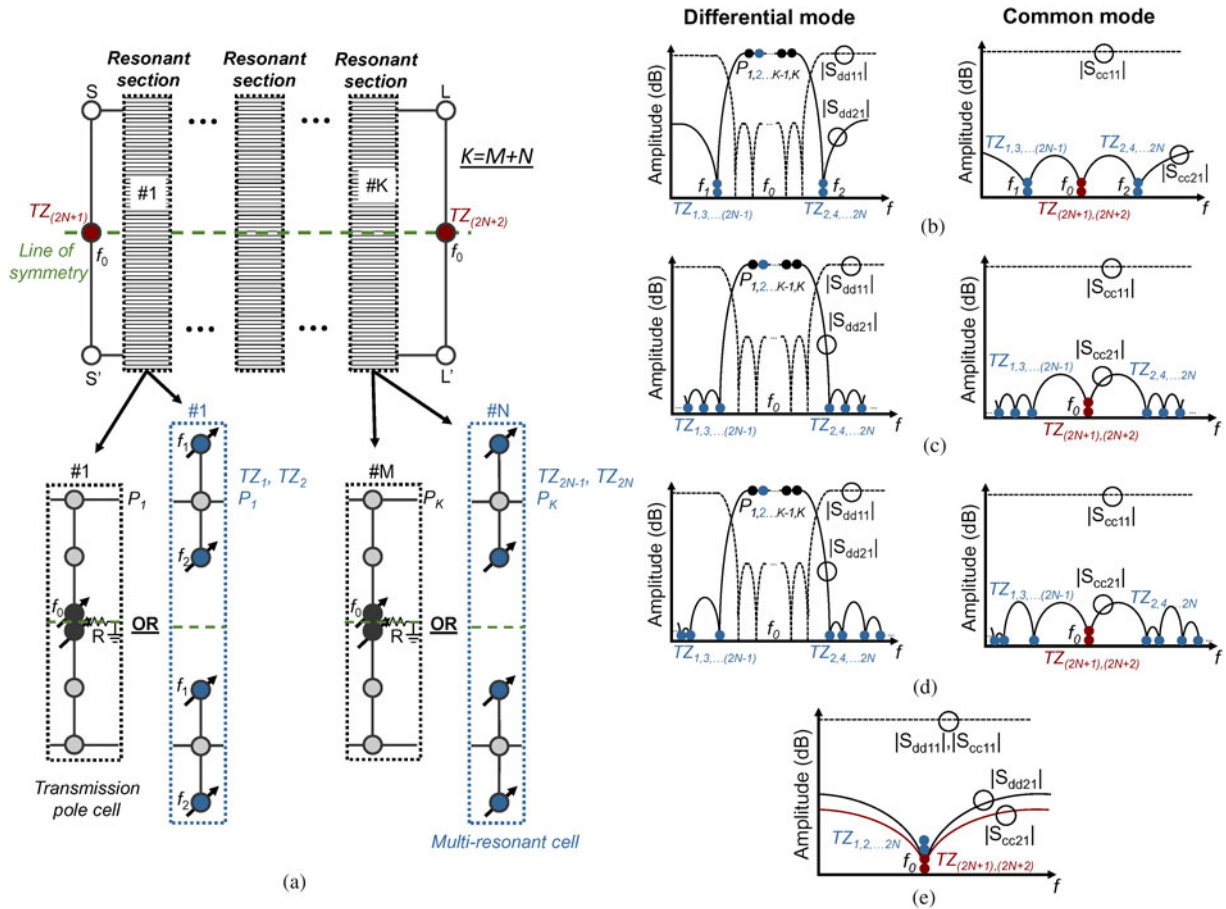
Fig. 1. Balanced BPF concept. (a) Overall CRD. White circles: sources and loads. Grey circles: non-resonating nodes. Black, red, and blue circles: resonating nodes. Black lines: static couplings. Differential and common-mode responses when; (b) TZs are placed at two frequencies, f_1 and f_2, (c) TZs are symmetrically spaced around passband, and (d) TZs are asymmetrically spaced around passband. (e) Intrinsic switching off of the filter.
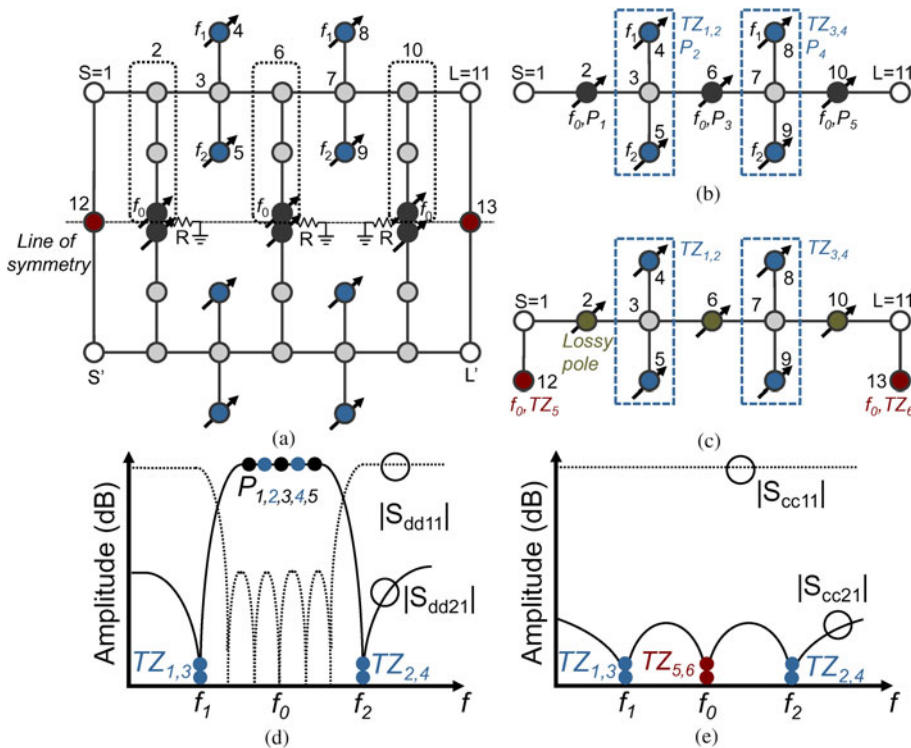

Fig. 2. Balanced BPF concept for $M = 3$, $N = 2$, and $K = 5$. (a) Overall CRD. (b) CRD equivalent of the differential mode. (c) CRD equivalent of the common mode. White circles: sources and loads. Grey circles: non-resonating nodes. Black, red, and blue circles: resonating nodes. Green circles: lossy resonating nodes. Black lines: static couplings. (d) Conceptual transfer function of the differential mode. (e) Conceptual transfer function of the common mode.
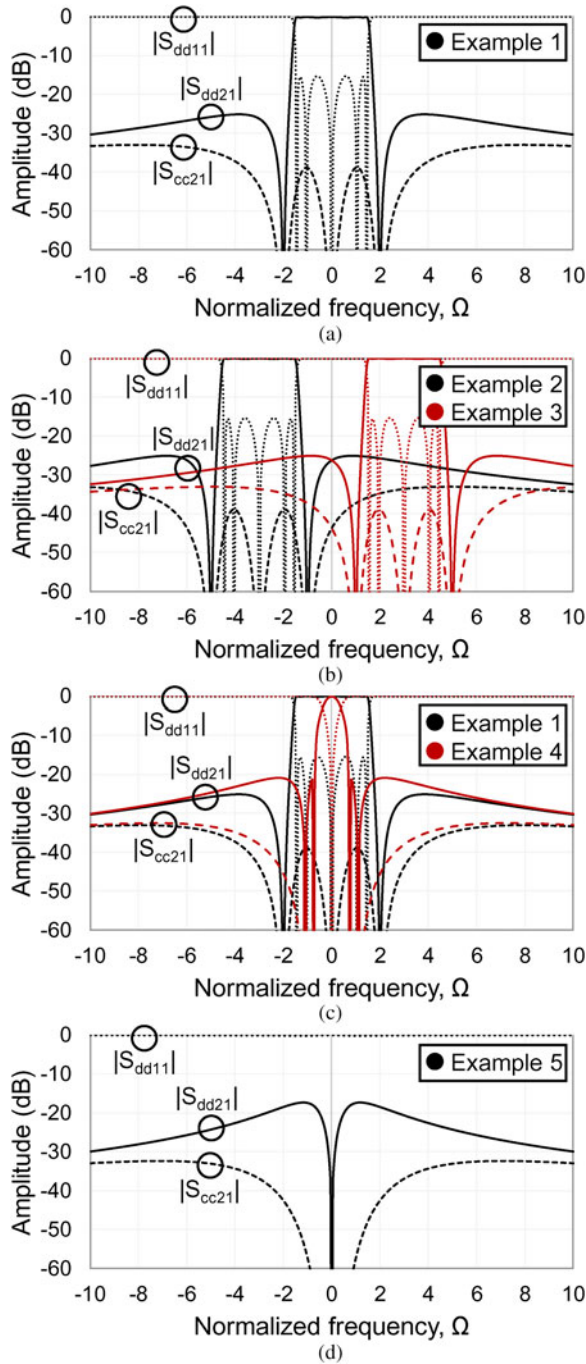
Table 1. Coupling coefficients of the examples in Fig. 3 associated to the CRDs in Fig. 2

Example	1	2	3	4	5
$M_{2,2}$	0	3	−3	0	0
$M_{4,4}$	2	5	−5	1.1	0
$M_{5,5}$	−2	1	−1	−1.1	0
$M_{6,6}$	0	3	−3	0	0
$M_{8,8}$	2	5	−5	0.72	0
$M_{9,9}$	−2	1	−1	−0.72	0
$M_{10,10}$	0	3	−3	0	0
$M_{12,12}$	0	3	−3	0	0
$M_{13,13}$	0	3	−3	0	0

For the common mode $−j \times 3.5$ is added to $M_{2,2}$, $M_{6,6}$, and $M_{10,10}$ to account for resistive loading. The rest of the coefficients are: $M_{1,2} = M_{10,11} = 1.4$, $M_{2,3} = M_{7,10} = 1.35$, $M_{3,6} = M_{6,7} = 1$, $M_{3,4} = M_{3,5} = M_{7,8} = M_{7,9} = 1$, $M_{1,12} = M_{11,13} = 2$.
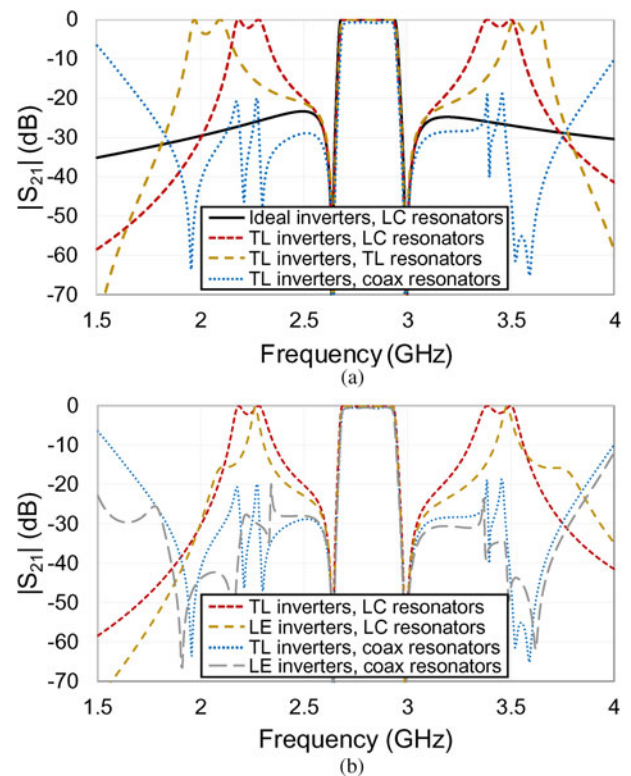

Fig. 3. Synthesized power transmission and reflection responses of the balanced BPF concept using the CRDs in (Figs 2(b) and 2(c)) and the coupling coefficients listed in Table 1. (a) Response of a single state. (b) Center frequency tuning. (c) BW tuning. (d) Intrinsic switching.

Fig. 4. Ideal power transmission responses of the differential mode as a function of inverter and resonator types. The responses are obtained by linear circuit simulations. (a) Comparison of types of resonators. (b) Comparison of types of inverters for two different resonators.

frequencies of the filter's resonators (as opposed to also adjusting its couplings). Specifically, the BW is determined by the separation of the TZs relative to the center frequency of the passband. This separation is varied by altering the resonant frequencies of the resonators in the MRCs. As an additional benefit of this filter architecture, intrinsic switching off can be achieved by setting all resonators to resonate at the same frequency, as is shown in Fig. 3 (d). As it can be seen, no transmission of signals is allowed in both

the differential and common modes of operation and the filter essentially acts as a switch in the off position.

Practical design aspects

It is important to consider practical design aspects when developing a physical filter based on a CRD. For example, CRDs are conventionally realized by replacing the resonating nodes with LC
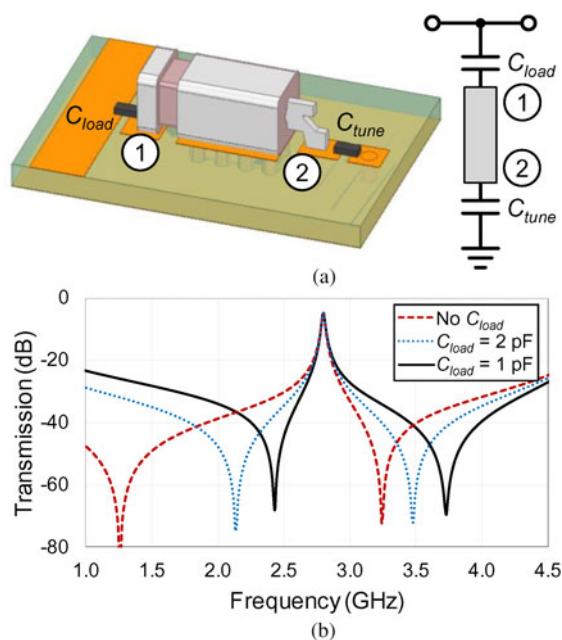
Fig. 5. Capacitively loaded ceramic coaxial resonator concept. (a) Three-dimensional model and circuit equivalent. (b) Power transmission response for alternative C_{load} values that result in TZ reallocation. In all responses $C_{tune} = 1.4$ pF.
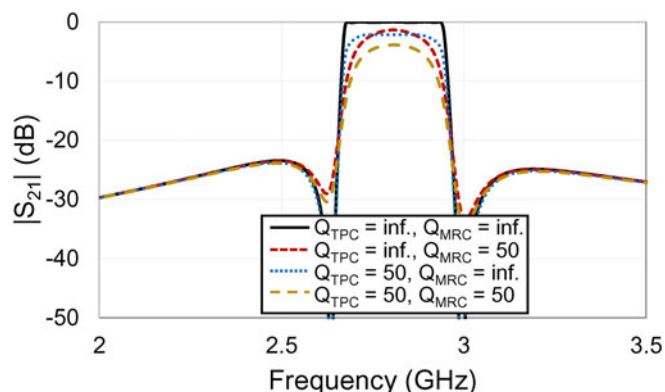

Fig. 6. Loss analysis of the balanced BPF. Two groups of resonators are considered: (i) MRC resonators with quality factor Q_{MRC} and (ii) TPC resonators with quality factor Q_{TPC}.

Fig. 7. Power transmission response of the CRD in Fig. 2(b) when the TPC resonators are replaced by EM-simulated coax or microstrip resonators and are loaded with lossy capacitors ($Q = 50$) that resemble the loss of the varactor.

Fig. 8. Ideal power transmission responses when using ceramic coaxial resonators and all TZs have been split to increase out-of-band spurious response rejection. (a) Differential mode. (b) Common mode.

resonators and the coupling elements with impedance or admittance inverters. However, there are a number of different resonators and inverter types (lumped element (LE), microstrip, coax, waveguide, etc.) that could be used in the physical design process. To compare the effects of different types of resonators and inverters, the resulting differential mode responses of various combinations of the inverter (ideal, TL, and LE) and resonator (LC, TL, and coaxial ceramic) types are shown in Fig. 4. In particular, Fig. 4(a) compares the responses of the balanced BPF when ideal inverters and LC resonators are used to when 90°-long TL-based inverters are implemented. As can be seen, the distributed nature of the TL-based inverters results in additional spurious peaks at both the lower and upper sides of the passbands. A potential solution to lowering the spurious peaks is to use LE inverters, which are not distributed and can be realized by either their lowpass or highpass π-type equivalent. This can be seen in
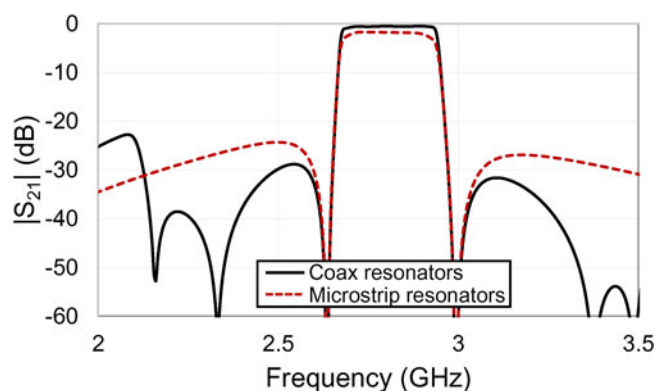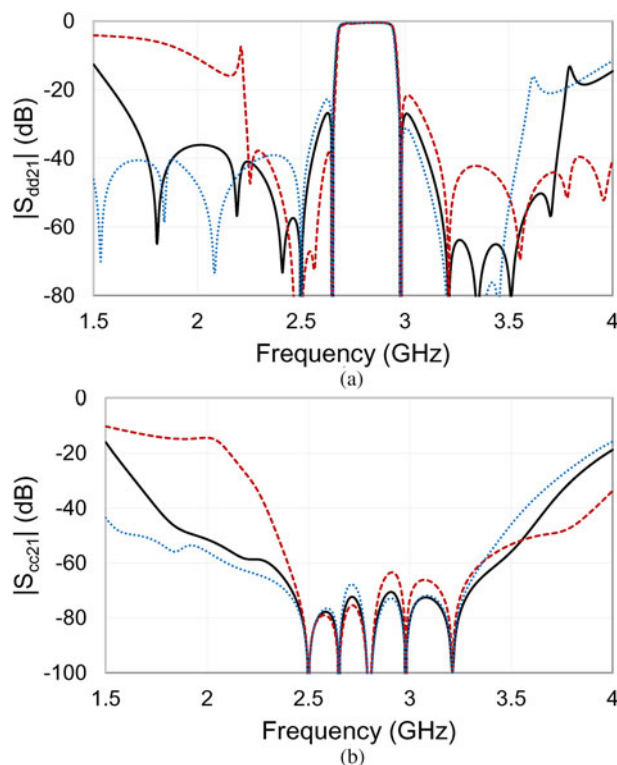
Fig. 4(b) where the balanced BPF has been implemented with TL and LE inverters for two different types of resonators (LE tanks and coaxial ceramic resonators). It can be observed that for both types of resonators, the LE inverters result in lower spurious peaks. Specifically, a mixture of lowpass type and highpass type inverters were used in the examples of Fig. 4(b) in order to equally suppress the peaks on both sides of the passband.

Figure 4 considers cases where coaxial type resonators have been used in an attempt to further reduce the spurious peaks present in the balanced BPF by introducing additional TZs. In these cases, a hybrid integration scheme, in which capacitively loaded
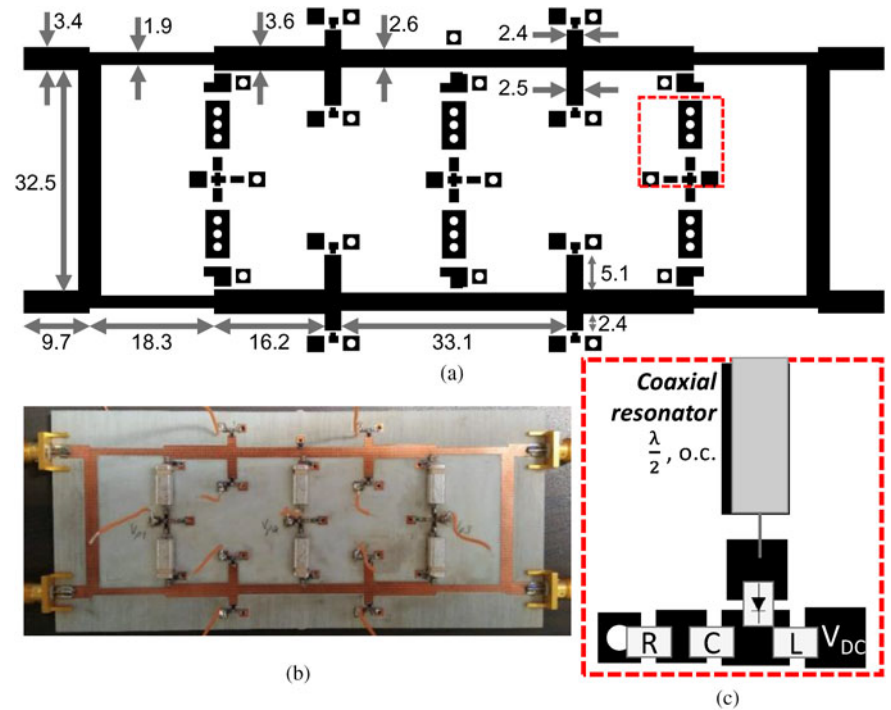
Fig. 9. Manufactured prototype. (a) Layout with dimensions in millimeters. (b) Photograph. (c) Close-up of the DC biasing network of the varactor diodes.

ceramic coaxial resonators were used in the TPCs (nodes 2, 6, and 10) and quarter-wavelength-long microstrip-based resonators were used in the MRCs (nodes 4, 5, 8, and 9), was considered. The ceramic coaxial resonator concept is shown in Fig. 5 and has also been discussed in [14] but for the design of reflectionless-type filters. It is based on commercially available resonators that are open-ended and half-wavelength-long at their resonant frequency. Such resonators have advantages in terms of quality factor (>400) and size compactness (due to high-dielectric constants). Additionally, their response can be exploited to further cancel the spurious bands in the differential mode by using their additional series-type quarter-wave resonances, which result in TZs. As shown in Fig. 5, the capacitor, C_{load}, capacitively loads the input of the resonator and its value determines the locations of these additional resonances and, therefore, the resulting TZs. Moreover, the capacitor, C_{tune}, capacitively loads the output of the resonator and controls the main half-wave resonance of the resonator.

The ceramic resonators have been used in the TPCs due to: (1) their size integration benefits, (2) their quality factor being higher than microstrip resonators, and (3) the fact that each of them results in two controllable TZs in the out-of-band response that enhance the filter selectivity. To corroborate the advantages of the proposed approach, Fig. 6 compares the ideal response of the balanced filter when different quality factors are considered for the two types of cells. Specifically, the MRCs have quality factor Q_{MRC} and the TPCs have quality factor Q_{TPC}. A quality factor of 50 is chosen as a value because it is representative of the varactors that operate at this frequency range. As it can be seen, the response has less insertion loss (IL) (1.4 dB compared to 2.2 dB) when lossy resonators are used for the MRCs than when they are used for the TPCs. This is because the poles from the MRCs are a result of a phase cancellation and therefore they are not directly influenced by the loss in the resonators. Furthermore, Fig. 7 illustrates the IL benefits of using ceramic

coaxial resonators in the TPC as opposed to a conventional approach using 90°-long microstrip type resonators. The illustrated responses have been obtained by linear simulations of the single-ended filter in Fig. 2(b), where the TPC resonators have been implemented with EM-simulated coaxial or microstrip resonators that are loaded with lossy capacitors ($Q = 50$). With all else equal, the filter implemented with coaxial resonators has noticeably less IL (0.4 dB) compared to the filter that uses microstrip resonators (1.7 dB).

As shown in Fig. 5, the TZs introduced by the coaxial resonators can either be symmetrically or asymmetrically arranged around the main resonance. Therefore, each ceramic resonator that is used in the filter can have its own unique TZ locations (i.e., all ceramic resonators have different C_{load} values) or all TZs can be placed at the same frequencies (i.e., all resonators have the same C_{load} value). In total there are ten TZs present in the differential mode response, four from the MRCs and six from the TPCs. If it is desired that all TZs be separated, the C_{load} for each coaxial resonator must be different and nodes 4, 5, 8, and 9 must have different resonant frequencies. Figure 8 shows a few potential ideal transfer functions when these conditions are met and all ten TZs are separated in frequency. For example, the TZs can be placed in order to reduce transmission on both sides of the passband equally (black trace) or placed in order to focus the reduction on one side or the other (red and blue traces). As can be seen in Fig. 8(b), the common mode has six TZs (two are located at the center frequency). The other TZs that result from the ceramic coaxial resonators have only little effect on the common-mode response, as the resonators are resistively loaded in that mode.

Experimental validation

In order to experimentally validate the proposed balanced BPF concept, a mixed-technology prototype was designed at 2.7 GHz
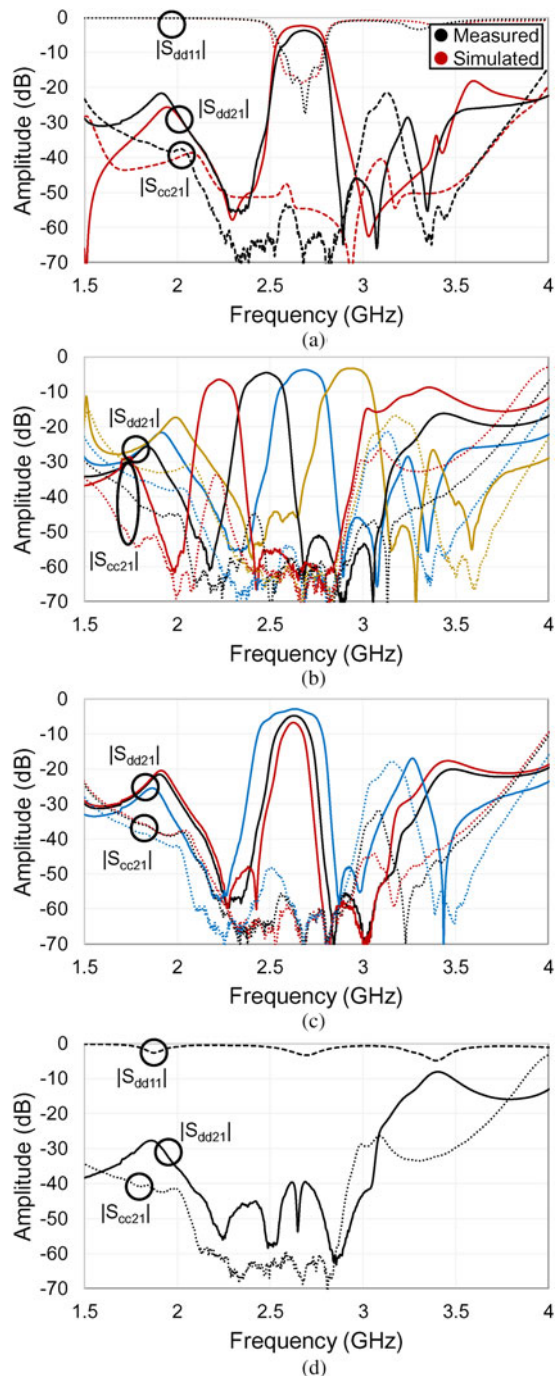
Fig. 10. Measured power transmission and reflection responses of the prototype in Fig. 9. (a) Comparison of EM-simulated and RF-measured states. (b) Center frequency tuning. (c) BW tuning. (d) Intrinsic switching off.

for a nominal fractional BW of 10% (270 MHz). The details of the manufactured prototype are shown in Fig. 9. It was designed and built on a Rogers RO4003C substrate (relative permittivity $\varepsilon_r = 3.38$, dielectric thickness $H = 1.52$ mm, and dielectric loss tangent $\tan(\delta_D) = 0.0027$). The resonators in the MRCs were incorporated with their connecting impedance inverters and were equivalently realized with quarter-wavelength long microstrip lines. They were then capacitively loaded with varactor diodes to tune their resonant frequencies. The TPCs were realized with ceramic coaxial

resonators from Integrated Microwave Corp [15], which are capacitively loaded at their inputs with static capacitors (to set the resulting TZs) and with varactor diodes at their outputs (to enable resonant frequency tuning). The varactor diodes are from Skyworks Inc. (model SMV1405). As shown in Fig. 9(c), the biasing network for providing DC voltage to the varactor diodes consists of an RF-choke inductor, L, and a DC-blocking capacitor, C.

The measured responses of the prototype are shown in Fig. 10. In particular, Fig. 10(a) compares one RF-measured state and one EM-simulated state, which appears to be in fair agreement. As it is shown, the balanced filter results in a highly selective transfer function and suppresses the common mode by ~70 dB at the center of the passband and by >50 dB in the range of 2.14–2.94 GHz (i.e., 1.4:1 ratio). In Fig. 10(b) the measured center frequency tuning states are shown. The filter can be tuned in terms of center frequency from 2.22 to 2.94 GHz, a ratio of 1.32:1, while maintaining a common-mode suppression of at least 35 dB at the center frequency and within a wide frequency range. The BW tuning of the filter is experimentally corroborated in Fig. 10(c). Its differential mode BW can be tuned from 104 MHz (4%) to 268 MHz (10.1%), a ratio of 2.58:1. The common mode is suppressed by at least 50 dB throughout this tuning range. In the aforementioned tuning states, the measured minimum in-band IL of the differential mode varies between 2.9 and 6.8 dB. Most of this loss can be attributed to the varactors, which have a quality factor of around 50 at 2.8 GHz. Lastly, the filter is intrinsically switched off so that no transmission is allowed in both the common and differential modes in Fig. 10(d). The differential mode transmission is suppressed by over 50 dB at the center frequency and by over 20 dB from 1.14 to 3.16 GHz, a 2.8:1 ratio.

Table 2 compares the filter presented in this paper with others in the state of the art [2–12]. As it can be seen, the filter presented in this work exhibits the highest selectivity in the differential mode (ten TZs and five poles, as opposed to two TZs and three poles in the next closest) and has the highest number of TZs in the common mode (6). Furthermore, it has an intrinsic switching capability. Compared to the work in [12], the filter in this paper is more selective and it has a higher number of poles and TZs. Moreover, it is tuned electronically using commercially available varactors as opposed to mechanically tuned capacitors in [12]. Lastly, this manuscript demonstrates how the proposed concept can be scaled to high-order transfer functions with a large number of TZs in the out-of-band response of the differential mode and a large number of TZs within the common-mode suppression BW.

Conclusion

This paper reported on a new class of high-order fully reconfigurable balanced BPF that uses both coaxial and microstrip type resonators. The proposed concept was presented through CRD and circuit-based examples that expound upon its design and operating principles. The balanced filter is tuned by only varying its constituent resonators' resonant frequencies and results in high levels of tunability in terms of center frequency, BW, and intrinsic switching off. Throughout all theoretical and experimental examples, the common mode is suppressed highly due to additional TZs and resistive loss that are only present in the common mode. Furthermore, the coaxial resonators, used in the hybrid-integration scheme, result in additional resonances that introduce TZs to suppress out-of-band spurious responses.

Table 2. Comparison with state of the art

Ref.	f_{cen}, GHz	BW, MHz	DM IL, dB	CMS at f_{cen}, dB	CM TZs	DM TZs	DM poles	IS
[2]	1.60–2.27 (1.42:1)	137	2.0–4.2	30–35	0	2	2	No
[3]	7.31–7.62 (1.04:1)	~200	1.3	20–25	0	2	2	No
[4]	1.03–1.55 (1.50:1)	85	1.8–3.9	50–70	1	2	2	No
[5]	0.66–0.96 (1.45:1)	~100	1.6	60–65	0	0	1	No
[6]	0.84–1.15 (1.37:1)	~100	1.6–2.7	50–65	0	1	2	No
[7]	0.97–1.72 (1.77:1)	80	3.0–4.5	30–50	0	0	2	No
[8]	0.73–1.60 (2.19:1)	95	2.5–5.7	40–50	0	1	2	No
[9]a	1.17–1.92 (1.64:1)	140	2.9–6.0	35–60	1	2	3	No
[9]b	0.55–0.78 (1.42:1)	60	3.5–4.2	40–60	1	1	3	No
[10]	0.58–1.22 (2.10:1)	65–180 (2.77:1)	1.8–4.6	30–55	0	1	2	No
[11]	0.80–1.52 (1.90:1)	63–140 (2.22:1)	2.4–5.8	20–35	0	1	2	No
[12]	1.36–1.90 (1.40:1)	43–270 (6.28:1)	0.8–3.5	40–70	4	2	3	Yes
This	2.22–2.94 (1.32:1)	104–268 (2.58:1)	2.9–6.8	35–65	6	10	5	Yes

f_{cen}, center frequency; DM, differential mode; CM, common mode; CMS, common-mode suppression; IS, intrinsic switching.

For experimental validation, an electronically tunable, mixed-technology microstrip prototype was manufactured and measured at S-band. It demonstrated center frequency tuning in a 1.32:1 ratio, BW tuning in a 2.58:1 ratio, and a highly suppressed common mode (>50 dB) throughout all tuning measurements.

References

1. **Feng W, Che W and Xue Q** (2015) The proper balance: overview of microstrip wideband balanced circuits with wideband common mode suppression. *IEEE Microwave Magazine* **5**, 55–68.
2. **Zhou WJ and Chen JX** (2017) High-selectivity tunable balanced bandpass filter with constant absolute bandwidth. *IEEE Transactions on Circuits and Systems II: Express Briefs* **8**, 917–921.
3. **Zhang H, Kang W and Wu W** (2018) Balanced bandpass filter with tunable centre frequency based on substrate integrated waveguide technology. *Electronics Letters* **14**, 886–888.
4. **Deng H, Sun L, Liu F, Xue Y and Xu T** (2019) Compact tunable balanced bandpass filter with constant bandwidth based on magnetically coupled resonators. *IEEE Microwave and Wireless Components Letters* **4**, 264–266.
5. **Zou XT, Wei F, Zhou B, Li B and Shi XW** (2018) Compact tunable balanced bandpass filter using a folded S-shaped slotline resonator (FSSR), Intern. Conf. on Microw. and Milli. Wave Tech., Chengdu, China.
6. **Zhao XL, Gao L and Xu JX** (2015) Tunable balanced bandpass filter with high common-mode suppression. *Electronics Letters* **24**, 2021–2023.
7. **Song K, Wang X, Fan M, Chen Y, Patience SR, Iman AM and Fan Y** (2020) Tunable balanced bandpass filter with constant absolute bandwidth and high common mode suppression. *IET Microwaves, Antennas & Propagation* **2**, 147–152.
8. **Mao J, Che W, Ma Y and Chen J** (2014) Tunable differential-mode bandpass filters with wide tuning range and high common-mode suppression. *IET Microwaves, Antennas & Propagation* **6**, 437–444.
9. **Li YC and Xue Q** (2011) Tunable balanced bandpass filter with constant bandwidth and high common-mode suppression. *IEEE Transactions on Microwave Theory and Techniques* **10**, 2452–2460.
10. **Zhu H and Abbosh AM** (2016) Tunable balanced bandpass filter with wide tuning range of center frequency and bandwidth using compact coupled line resonator. *IEEE Microwave and Wireless Components Letters* **1**, 7–9.
11. **Zhang SX, Chen ZH and Chu QX** (2017) Compact tunable balanced bandpass filter with novel multi-mode resonator. *IEEE Microwave and Wireless Components Letters* **1**, 43–45.
12. **Simpson DJ and Psychogiou D** (2018) Coupling matrix-based design of fully reconfigurable differential/balanced RF filters. *IEEE Microwave and Wireless Components Letters* **10**, 888–890.
13. **Simpson D and Psychogiou D** (2020) High-order fully-reconfigurable balanced bandpass filters using mixed technology resonators, European Microwave Conference, Utrecht, The Netherlands.
14. **Simpson D, Gómez-García R and Psychogiou D** (2021) Hybridly-integrated quasi-elliptic-type bandpass filters with symmetrical quasi-reflectionless characteristics, International Microwave Symposium, Atlanta, GA, USA.
15. **Integrated Microwave Corporation website** (2002) [Online]. Available at http://www.imcsd.com.

Dakotah Simpson was born in Thornton, Colorado, USA in 1994. He received the B.S. and M.S. degrees in Electrical Engineering from the South Dakota School of Mines and Technology, Rapid City, South Dakota, in 2017 and the University of Colorado Boulder, Colorado, in 2020, respectively. He is currently pursuing his Ph.D. degree in Electrical Engineering at the University of Colorado Boulder. His current research interests include the design, characterization, and synthesis of reconfigurable microwave single-ended and balanced filters and frequency selective feed networks for linear antenna arrays. Simpson is a member of the IEEE Microwave Theory and Techniques Society (IEEE MTT-S) and the Applied Computational Electromagnetics Society (ACES). He is the recipient of the MTT-S 2018 Graduate Fellowship, the University of Colorado's Dean's Graduate Assistantship and the ECEE Gold Award for Research.

Dimitra Psychogiou received the Dipl.-Eng. degree in Electrical and Computer Engineering from the University of Patras, Patras, Greece, in 2008 and the Ph.D. degree in Electrical Engineering from the Swiss Federal Institute of Technology (ETH), Zürich, Switzerland, in 2013. She is currently a Professor of Electrical and Electronic Engineering at the University College Cork (UCC) and the Tyndall National Institute, Cork Ireland. Prior to joining UCC, she was a Sr. Research Scientist with Purdue University, West Lafayette, IN, USA and an Assistant Professor with the University of Colorado Boulder, Boulder, CO, USA. Her current research interests include RF design and characterization of reconfigurable microwave and millimeter-wave passive components, RF-MEMS, acoustic wave resonator-based filters, tunable filter synthesis, and frequency-agile antennas. Her research has been presented in more than 160 IEEE publications and has received the 2020 CAREER award from the National Science Foundation (NSF), the 2020 URSI Young Scientist Award and the Junior Faculty Outstanding Research Award from UC Boulder. Professor Psychogiou is a Senior Member of IEEE and URSI and a member of the *IEEE MTT-S Filters and Passive Components (MTT-5)* and *Microwave Control Materials and Devices (MTT-13)* committees. Furthermore, she serves on the Technical Review Board of various IEEE and EuMA conferences and journals and is the Chair of MMT-13 and the Secretary of the USNC-URSI Commission. She is an Associate Editor for the *IEEE Microwave and Wireless Components Letters* and the *International Journal of Microwave and Wireless Technologies*. Previously, she was an Associate Editor of the *IET Microwaves, Antennas, and Propagation Journal*.